Polarization Selective Transparent Electrode With Patterned Metal for the 3D Display Pixel

Young Jin Jung and Namkyoo Park

***Abstract*—We propose a polarization selective transparent electrode (PSTE) utilizing a rectangular-shaped metal nano-wire structure. The performance of the PSTE was evaluated with simulation based on finite element method (COMSOL Multiphysics). Parametric studies have been carried out to give a guide for geometric parameter selection to meet the requirement of the target application. According to the studies, 70 nm by 800 nm rectangular metal grid, having a thickness of 100 nm and linewidth of 30 nm were recommended to keep higher than 61% transmittance, 24 dB extinction ratio, and lower than 5 Ω/sq sheet resistance. As an application of PSTE, a design idea about crosstalk reduction of the passive stereoscopic 3D display is proposed by presenting its pixel structure employing the proposed PSTE. The light extraction efficiency of the proposed pixel employing PSTE structure was also evaluated and compared to the structure employing the lossless ITO (Indium Tin Oxide), by measuring extracted light output power from incoherently distributed dipole sources excited in the emission layer. Degradation of the extraction efficiency below 14 percent point was expected compared to the lossless ITO for all the primary color wavelength range.**

***Index Terms*—3D-display, patterned metal, polarizer, transparent electrode.**

I. Introduction

METAL wire-grid polarizers is consist of parallel metal wires spaced by a period of less than sub wavelength. If the wire width is smaller than sub wavelength, free electrons cannot oscillate in the perpendicular while it can oscillate along wire direction. Therefore, perpendicularly polarized light (to wire direction) can pass through the layer while parallel polarized light is reflected as flat metal surface when wire interval is narrow enough. It has attracted much attention due to their various advantages over absorptive polarizers based on PVA (polyvinyl alcohol). Most of all, with its excellent compatibility in integration with the fabrication process of semiconductor devices, for example, embedded metal wire-grid polarizer in the light emitting diode can be realized, for better optical efficiency [1], [2]. In liquid crystal display applications, better efficiency display has been reported by reusing reflected unpolarized photons from the wire-grid polarizer [3], [4]. With its extreme device tolerance for temperature and photon flux, applications for the projection display also have been considered attractive [5], [6]. Not limited to the optical frequency and display application, it is noted that wire grid polarizer structures also can are used in the infrared/terahertz application with appropriate design of grid periods [7]–[9].

On the other hand, there have been serious efforts on new types of transparent electrodes to overcome ITO's (Indium Tin Oxide) mechanical stiffness hindering its applications for the flexible devices [10]–[12], and as well to avoid the material supply-cost issues of ITO [10]. Transparent electrodes based on CNT (carbon nanotubes) [10], [13]–[16], graphene [10], [17]–[21] and metal nanostructure (aligned wires or grid) [10], [13], [14], [22]–[29] or their hybrid structures [17] has been studied as an alternative to ITO. Among these alternatives, especially, metal nanostructure can give more functions (such as polarization control) by designing metal pattern while overcoming ITO's disadvantages mentioned earlier [10], [13].

In this paper, motivated by the common factor between two devices, specifically, the use of metals in the transparent electrode and the metal wire-grid in the polarizer, we propose a device of integrated functionality: polarization selective transparent electrode (PSTE). The domains of optimal design for the PSTE are investigated utilizing FEM (Finite-Element Method) in terms of transmittance, polarization extinction ratio, and sheet resistance, by adjusting the period, aspect ratio, fill factor and thickness of rectangular metal mesh. Out of various possible applications of PSTE, crosstalk reduction for the passive stereoscopic 3D display is proposed and analyzed. The extraction efficiency of the proposed display pixel employing PSTE was also evaluated by comparing it with the lossless ITO.

II. Crosstalk in Passive Stereoscopic 3D Display and Proposed Solution

Passive stereoscopic 3D display based on polarized light is one of the most popular commercialized 3D displays. Compared to the active time division 3D stereoscopic display, it also has some distinctive advantages. A liquid crystal shutter in glasses and the display-panel are not necessary, and a passive stereoscopic 3D display does not experience the ambient sync issues between 3D glasses and the display panel as a public display [30]. However, one of the significant disadvantages of

Manuscript received June 26, 2021; revised August 21, 2021; accepted September 3, 2021. Date of publication September 8, 2021; date of current version September 23, 2021. This work was supported by the National Research Foundation of Korea through the Global Frontier Program under Grant GFP, 2014M3A6B3063708 funded by the Korean Government. *(Corresponding author: Young Jin Jung.)*

Young Jin Jung is with the School of Electricity and Electronics, Ulsan College, Ulsan 44610, Korea (e-mail: yjjung1980@gmail.com).

Namkyoo Park is with the Photonic Systems Laboratory, Department of Electrical and Computer Engineering, Seoul National University, Seoul 08826, Korea (e-mail: nkpark@snu.ac.kr).

Digital Object Identifier 10.1109/JPHOT.2021.3110986

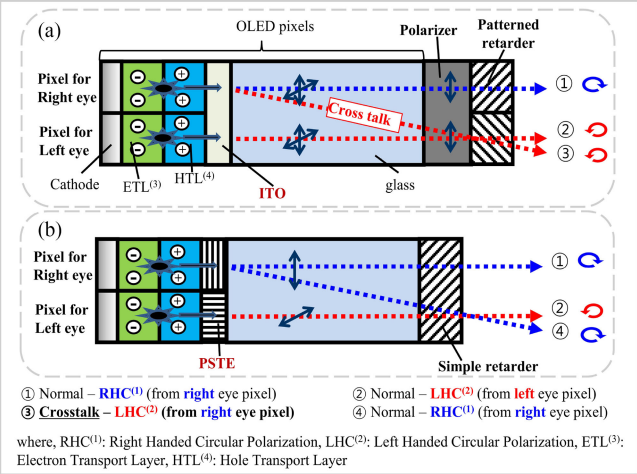

Fig. 1. (a) Schematic diagram of the passive 3D stereoscopic OLED display pixels employing conventional transparent conductive electrode (ITO) and illustration of their induced crosstalk. (b) Schematic diagram of the passive stereoscopic 3D OLED display pixels employing proposed PSTE. Crosstalk is not caused by the large distance between optical source and the retarder.

the commercial passive 3D display is the narrow vertical viewing angle caused by crosstalk due to the gap between pixels and the patterned retarder [31].

Fig. 1(a) shows the schematic diagram of the conventional passive stereoscopic 3D display pixels. Each pixel for the left and right eyes emits lights of orthogonal polarizations: usually of right and left-handed circular polarizations, to cope with the rotation of analyzing polarizers in the 3D eyeglass. As can be seen in Fig. 1(a), the output state of the circular polarization is usually achieved with the combination of a polarizer and patterned retarder (quarter wave plate). Optical axis of the retarder is patterned with 90 degrees offset aligned with corresponding eye pixels. Thereby, each left and right eye pixels emit corresponding circularly polarized light form the linealy polarized light [30], [31]. In this case, the SOP (state of the polarization) of the output is finally determined at retarder layer. It is worth mentioning that, therefore, a large distance between emitters and retarders causes crosstalk between left and right image as illustrated in Fig. 1(a). The distance can be decreased by grinding glass as thin as possible, but at the expense of extensive process and reliability issues [30]. The spatial separation of light paths between left and right pixels, with the use of partition walls (black matrix) of light absorbing material [30] also can be used, but with the reduction of the active area, and thus associated penalties in luminance and resolution of the display.

Fig. 1(b) shows the operation principle of proposed 3D display pixels to resolve the discussed difficulties in crosstalk, with the use of polarization selective transparent electrode. PSTEs of orthogonal linear polarizations are patterned on top of the left and right eye pixels, respectively. Upon the emission through each polarizer, each linearly polarized light is converted into left- and right-handed circular polarization, after passing through a simple retarder without patterning. If linearly -45° and +45° polarized light are obtained from pixels for left and right eye respectively with the help of patterned PSTE they can be expressed

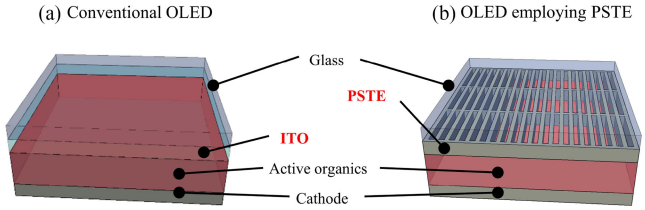

Fig. 2. Illustrations of OLED pixel structures (a) with conventional ITO, and (b) employing proposed PSTE as transparent electrode.

as (1). with Jones vectors.

$$\frac{1}{\sqrt{2}}\begin{bmatrix}1\\-1\end{bmatrix} \text{ and } \frac{1}{\sqrt{2}}\begin{bmatrix}1\\1\end{bmatrix} \tag{1}$$

And ach polarization state after passing through the simple retarder (quarter wave plate) can be expressed as (2) respectively.

$$\begin{bmatrix}1&0\\0&i\end{bmatrix}\frac{1}{\sqrt{2}}\begin{bmatrix}1\\-1\end{bmatrix} = \frac{1}{\sqrt{2}}\begin{bmatrix}1\\-i\end{bmatrix} \text{ and } \begin{bmatrix}1&0\\0&i\end{bmatrix}\frac{1}{\sqrt{2}}\begin{bmatrix}1\\1\end{bmatrix} = \frac{1}{\sqrt{2}}\begin{bmatrix}1\\i\end{bmatrix} \tag{2}$$

Therefore, left- and right-handed circular polarization can be obtained for each left and right eye. In this arrangement, meanwhile, it is possible to keep the final states of polarizations for each eye at the same state as the conventional 3D display pixels in Fig. 1(a), but since the split of polarization is achieved at the PSTEs in emitters' side, polarization crosstalk becomes independent of the emitter-retarder distance.

Fig. 2 illustrates OLED pixel structures using conventional ITO (corresponding to Fig. 1(a)) and employing proposed PSTE (corresponding to Fig. 1(b)). We assume a rectangular mesh of metal nanowires as the base design of transparent electrodes [13], [22]–[25], and take its dimension down to sub-wavelength scale to derive the functionality of a linear polarizer. Because the patterns of the metal are small enough to treat it as a metamaterial, microscopic pattern can be modified while keeping a role as an electrode.

III. Design of the PSTE

To get an intuition about designing PSTE as an electrode and at the same time as an optical polarizer for the target application, electrical sheet resistance, optical transmittance, and polarization extinction ratio (ER) were calculated.

A. Sheet Resistance

Fig. 3(a) illustrates the relationship between the sheet resistance and the resistance of the general conductive sheet. And the sheet resistance can be calculated as (3) [32].

$$R_s = \frac{\rho}{t} = R\frac{w}{l} \tag{3}$$

where, R, R_s and ρ are resistance measured along the length direction, sheet resistance under measurement and resistivity of the material, respectively. And, t, w and l are the thickness, width, and length of the structure, respectively.

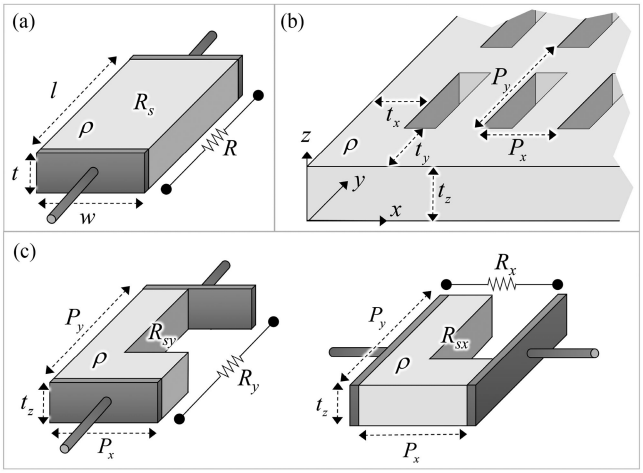

Fig. 3. (a) Illustration about relation between resistance and sheet resistance of general conductive sheet. (b) Schematic of the PSTE structure. (c) Illustration about calculation of average sheet resistance along each axis from the unit cell of structure of the PSTE.

It is worth mentioning that the PSTE is not an isotropic metamaterial for its electric properties due to its anisotropic structure as shown in Fig. 3(b). Therefore, the average sheet resistance of the PSTE is direction dependent. Fig. 3(c) illustrates how to calculate average sheet resistance along x-axis direction (R_{sx}) and y-axis direction (R_{sy}) by measuring the resistance of unit cell of PSTE. And the resistance of unit cell along each axis (R_x, R_y) can be calculated from the resistivity of the material. Unit cell structure can be treated as serially connected rectangular slab resistors and the resistance of unit cell can be calculated as (4), (5).

$$R_x = \rho\left(\frac{t_x}{t_z P_y}\right) + \rho\left(\frac{P_x - t_x}{t_z t_y}\right) = \frac{\rho}{t_z}\left(\frac{t_x}{P_y} + \frac{P_x - t_x}{t_y}\right) \tag{4}$$

$$R_y = \rho\left(\frac{t_y}{t_z P_x}\right) + \rho\left(\frac{P_y - t_y}{t_z t_x}\right) = \frac{\rho}{t_z}\left(\frac{t_y}{P_x} + \frac{P_y - t_y}{t_x}\right) \tag{5}$$

Where, t_x, t_y and t_z are the linewidth along x, y-axis direction and the thickness of the metal respectively, P_x, P_y are the period of mesh along each axis, and ρ is the resistivity of the metal (Al) used for the electrode (in this study, $\rho = 2.733 \times 10^{-8}$ Ω•m [33]). Therefore, the sheet resistance can be calculated as (6), (7) with (3).

$$R_{sx} = R_x \frac{P_x}{P_y} = \frac{\rho P_x}{t_z P_y}\left(\frac{t_x}{P_y} + \frac{P_x - t_x}{t_y}\right) \tag{6}$$

$$R_{sy} = R_y \frac{P_y}{P_x} = \frac{\rho P_y}{t_z P_x}\left(\frac{t_y}{P_x} + \frac{P_y - t_y}{t_x}\right) \tag{7}$$

Fig. 4 shows the calculated sheet resistance R_{xs} and R_{ys} as a function of period P_x and P_y, with thickness (t_z) and linewidth ($t_x = t_y$) detuning. As can be seen in Fig. 4, the sheet resistance along each axis (R_{xs}, R_{ys}) is mainly determined by the period of the metal grid (P_y, P_x) along the orthogonal axis at a fixed metal linewidth and thickness. And, lower sheet resistance can be achieved by increasing thickness or linewidth as can be seen in Fig. 4, but it may reduce transmittance as will be shown in the following chapter.

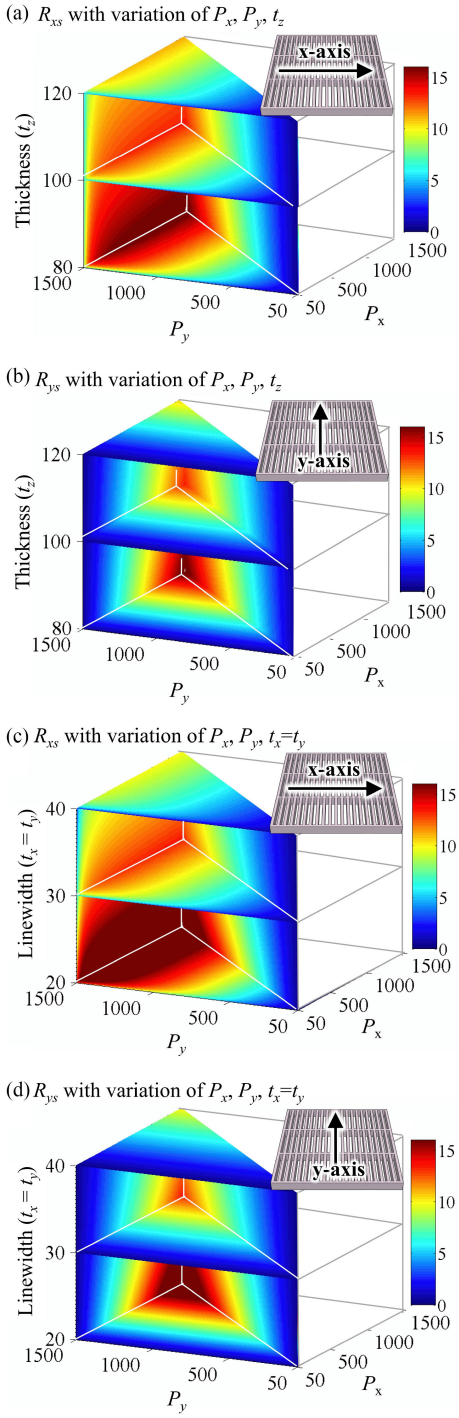

Fig. 4. (a) and (b) shows sheet resistance along x-axis (R_{xs}) and y-axis (R_{ys}) respectively as a function of mesh period (P_x, P_y) and thickness (t_z) at fixed linewidth ($t_x = t_y = 30$ nm). (c) and (d) shows sheet resistance along x-axis (R_{xs}) and y-axis (R_{ys}) respectively as a function of mesh period and linewidth at fixed thickness ($t_z = 100$ nm).

It is emphasized that resistance less than 10 Ω/sq can be achieved when linewidth >30 nm and thickness >100 nm while

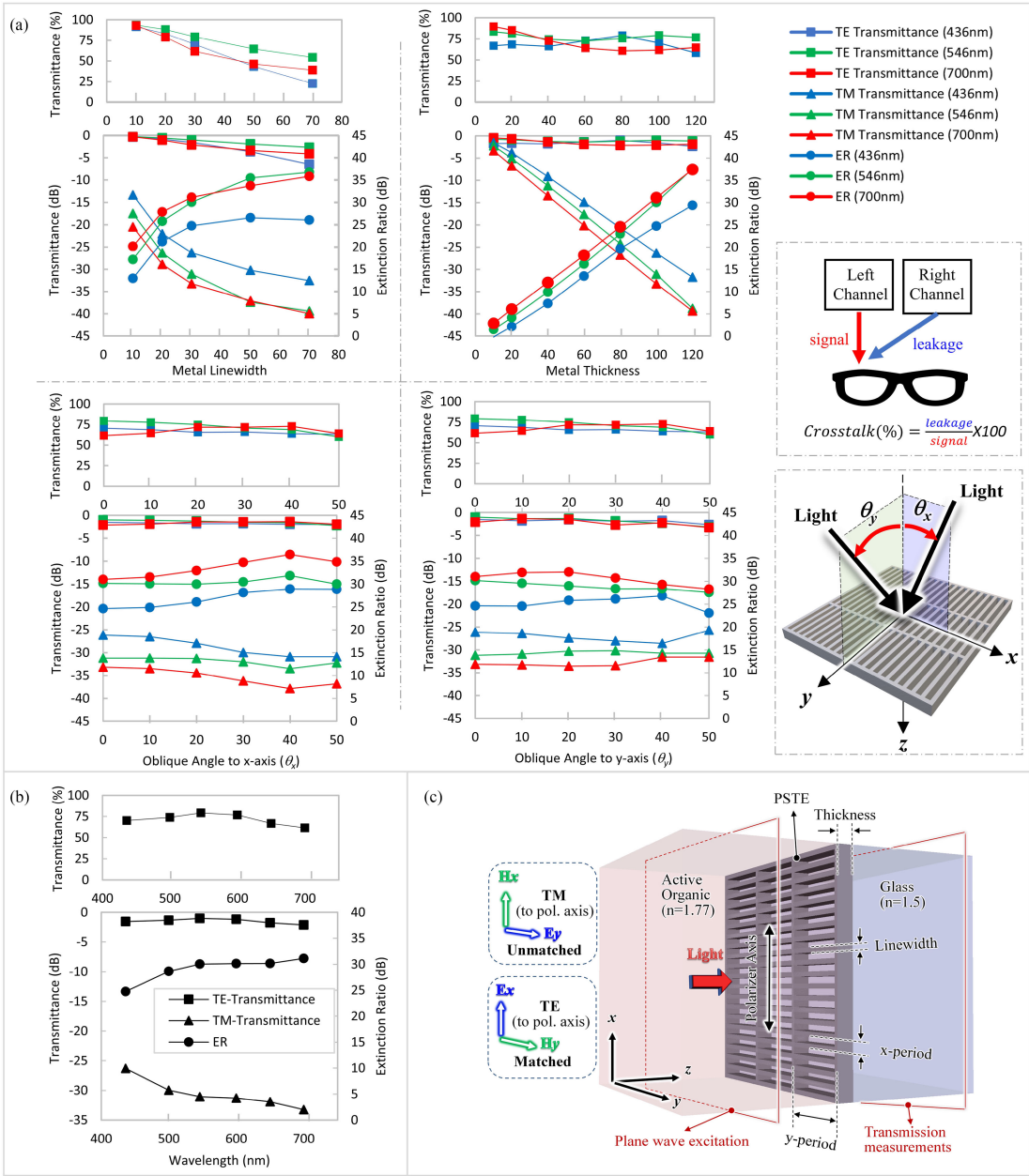

Fig. 5. (a) Transmittance and ER as a function of metal linewidth, thickness and angle of incidence and (b) as a function of wavelength. (ER= $10\log_{10}[T_{TE}/T_{TM}]$ dB where T_{TE} is TE wave transmittance and T_{TM} is TM wave transmittance). (c) Simulation setup for the calculation of the transmittance of PSTE.

keeping period below 1000 nm. And, it seems comparable to the high-quality ITO with the same thickness when considering the typical resistivity of ITO is $\sim 10^{-6}$ to 10^{-2} Ω•m [34].

B. Optical Transmittance and Polarization Extinction Ratio

Transmittance, and polarization ER must be optimized simultaneously by determining geometric parameters while considering fabrication tolerance to meet the needs of the target application. To observe optical transmittance and polarization ER simultaneously, FEM (Finite Element Method, COMSOL) was utilized while changing the geometric parameter of the structure. Fig. 5(c) illustrates the simulation setting for the proposed PSTE. Normally incident plane wave was excited in the organic layer, and the intensity of the transmitted light was measured in the glass layer. Space between metal wire grids was filled with organic material. For the fast convergence of the calculation, the initial solution of FEM was obtained from the dielectric structure without metal, and then the scattered field was calculated thereafter with the given PSTE structure under study. Periodic boundary conditions were set for four side surfaces perpendicular to the PSTE. And, PML (Perfectly Matched Layer) boundary conditions were used for the top and bottom surfaces of the simulation space. Tetrahedral mesh type was used with the grid size of less than 20 nm for metal, and 50 nm for other regions.

Left of Fig. 5(a) shows the simulation result of transmittance and ER for the three primary colors and each polarization, on the normal incidence of a plane wave, as a function of the metal linewidth ($t_x = t_y = 10 \sim 70$ nm) at fixed thickness ($t_z =$ 100 nm) and period ($P_x = 70$ nm, $P_y = 800$ nm) of PSTE. As can be observed from the results, there existed a trade-off between ER and transmittance, for the increase of metal linewidth. For increased metal linewidth, increased suppression of TM mode and higher ER was obtained. However, it should be noted that increased thickness results in a reduction of the polarization matched light transmittance (TE mode). Right of the Fig. 5(a) shows the transmittance and ER as a function of the metal thickness ($t_z = 10 \sim 120$ nm) at fixed linewidth ($t_x = t_y =$ 30 nm) and period ($P_x = 70$ nm, $P_y = 800$ nm) of PSTE. The tendency of transmittance and ER with thickness variation is similar to the case of linewidth variation but a slower change of transmittance and ER is observed in the case of the linewidth variation. Transmittance is decreased by loss inside the metal slit and assisted by plasmonic transmission through aperture opening. Losses are nearly proportional to the metal thickness and aperture opening is affected by linewidth variation. As can be seen, transmittance and ER is widely and easily adjustable with geometric parameters to achieve the performance for target application. But, in the case of PVA based polarizer, it is somewhat difficult to design because material treatments or mechanical stretching are required.

Angular dependency of the transmittance and ER for the three primary colors are shown in the lower side of the Fig. 5(a). Definitions of oblique angles (θ_x and θ_y are oblique angles to the x-axis and y-axis respectively) are shown in the right bottom corner of the Fig. 5(a). In the study, geometric parameters were set as $t_z = 100$ nm, $t_x = t_y = 30$ nm, $P_x = 70$ nm, and $P_y = 800$ nm where the common trend of the performance is actively changing. There are fluctuations of the TE transmittance $\sim$7.4% (blue)/$\sim$19.3% (green)/$\sim$11.4% (red) and ER $\sim$4.3 dB (blue)/$\sim$1.9 dB (green)/$\sim$5.4 dB (red) with the variation of θ_x from 0° to 50° (total internal reflection occur above critical angle 58° and surface treatment is required for wider viewing angle in practical application). And there are fluctuations of the TE transmittance $\sim$16.2% (blue)/$\sim$30.9% (green)/$\sim$26.5% (red) and ER $\sim$3.8 dB (blue)/$\sim$2.6 dB (green)/$\sim$3.8 dB (red) with the variation of θ_y from 0° to 50°.

As a point of view of 3D crosstalk, commercial companies set viewing angle of the display within 3D crosstalk of 7% [30]. And the 3D crosstalk can be defined as *leakage* over *signal* as illustrated in the right side of Fig. 5(a) [35]. It can be said that $\sim$11.5 dB is the minimum ER of the PSTE to meet crosstalk below 7% when considering (8). In this study, ER is above 23 dB at given geometric parameters as can be seen in Fig. 5(a). Therefore, the PSTE can expend viewing angle until other issues such as total internal reflection are happened. It can give much advantage when 16° viewing angle of conventional 3D display is considered [30]

$$\frac{leakage}{signal} = \frac{T_{TM}}{T_{TE}} < 7\% \tag{8}$$

TABLE I
PARAMETERS FOR THE CALCULATION

PARAMETERS		VALUES	PARAMETERS		VALUES
Metal linewidth	t_x	10 ~ 70 nm	Relative permittivity of Al [36] $\varepsilon_r = (n\text{-}ik)^2$	436 nm (Blue)	$(0.57\text{-}i5.14)^2$
	t_y	10 ~ 70 nm		546 nm (Green)	$(0.95\text{-}i6.36)^2$
Metal thickness	t_z	10 ~ 120 nm		700 nm (Red)	$(1.66\text{-}i8.04)^2$
Metal pattern period	P_x	60 ~ 800 nm	Refractive index	Glass	1.5
	P_y	60 ~ 200 nm		Organic	1.77
Organic layer thickness		250 nm		ITO	1.94
ITO thickness		100 nm	FEM Mesh type		Tetrahedral
Glass thickness		100 nm	Metal regions mesh size		< 20 nm
Cathode substrate thickness (*Al*)		100 nm	Dielectric regions mesh size		< 50 nm

To show the wavelength dependency of PSTE, Fig. 5(b) shows the transmittance and ER as a function of the wavelength (425 $\sim$ 700 nm) at arbitrary reliable geometric parameters. In the study, geometric parameters were set as $t_z = 100$ nm, $t_x = t_y = 30$ nm, $P_x = 70$ nm, and $P_y = 800$ nm. With the given geometric parameters, the transmittance of polarization matched light (TE-mode) higher than around 61% and ER higher than 24 dB is achievable for all the visible wavelength ranges.

To observe the dependency on mesh period (P_x, P_y) or duty cycle, a transmittance of the polarization matched light (TE mode), ER and sheet resistance were plotted simultaneously in Fig. 6 for the three primary colors respectively as a function of the period at the fixed metal thickness ($t_z = 100$ nm) and linewidth ($t_x = t_y = 30$ nm). Transmittance was plotted with the color-map. ER and sheet resistance was plotted with the red and blue lines, respectively. Sheet resistance only along x-direction was plotted because it is always larger than that of y-direction in the region of interest ($P_y > P_x$).

Geometric parameters can be selected to meet the overall performance requirements of the target application by referring to the presented study results while considering fabrication tolerance. For example, to keep transmittance higher than 61%, ER higher than 24 dB and sheet resistance below 5 Ω/sq, it is recommended that $P_x < 70$ nm and $P_y < 800$ nm at given thickness and linewidth ($t_z = 100$ nm, $t_x = t_y = 30$ nm).

C. Extraction Efficiency

Upon the parametric studies on the electrical and optical properties of the PSTE structure, its light extraction efficiency in an integrated OLED device was also estimated, assuming parameters listed in Table I. To take account of the incoherent Lambertian properties of OLED light, random phase, polarization, and location of each dipole source must be considered in the simulation. Random phase characteristics can be imitated by preventing coherent interference between nearby dipole sources. Therefore, only one dipole source must be excited at once

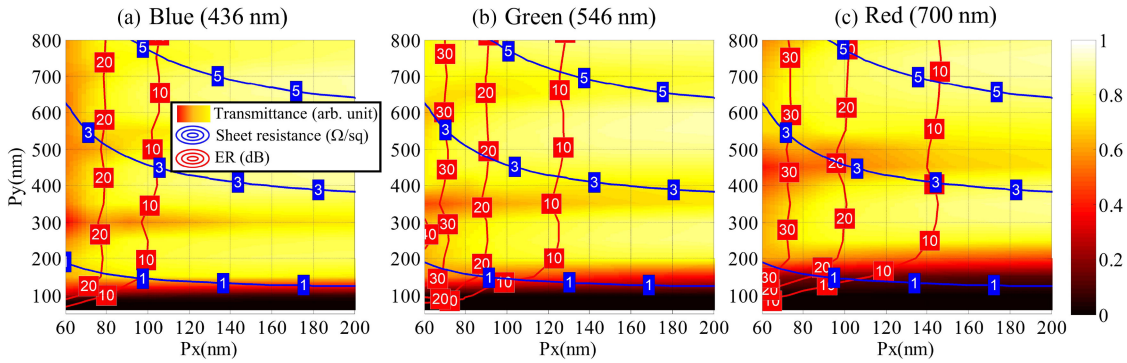

Fig. 6. Transmittance of polarization matched light (TE mode), ER and sheet resistance for the three primary colors as a function of the period (P_x, P_y) at fixed thickness ($t_z = 100$ nm) and fixed linewidth ($t_x = t_y = 30$ nm) of patterned metal. Transmittance was plotted with the color-map, ER and sheet resistance is plotted on the same layer with the red and blue lines, respectively.

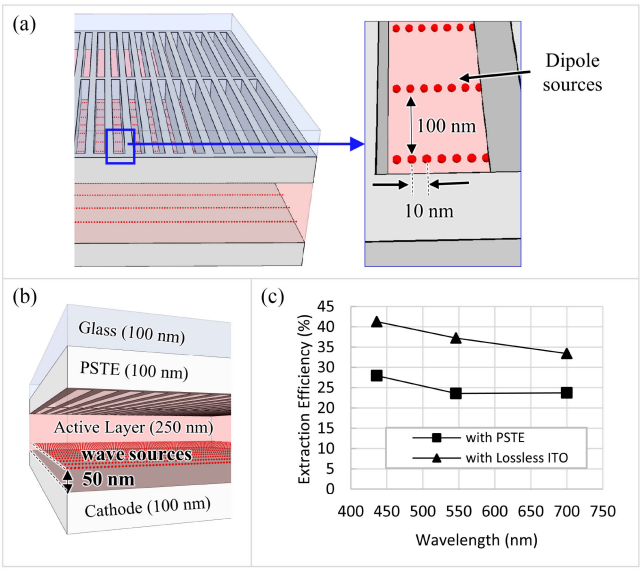

Fig. 7. (a) Schematics of the simulated structure with proposed PSTE indicating dipole source position and (b) layers. (c) Simulation results of the extraction efficiency of the OLED employing PSTE and lossless transparent electrode.

for each calculation of simulation. In addition, the extraction efficiency of each dipole source depends on its located position because the light from each dipole undergoes a different path while escaping from the OLED structure. Therefore, independent simulation must be carried out for all possible combinations of polarization and location. And the contribution of each dipole must be combined in a super-positional manner. In the simulation, x- and y-polarized current dipole sources were distributed in the active layer. And, they are placed 50 nm above the cathode with 10 nm and 100 nm intervals for x-axis and y-axis respectively as shown in Fig. 7(a) and (b). Dipole sources placed in a unit period is enough to estimate efficiency of the entire surface of the emission layer for the symmetricity. The extracted light from z-polarized light is negligible because the main radiation direction is parallel with the x-y plane and it is hard for z-polarized light to escape from the surface.

Fig. 7(c) shows the obtained OLED extraction efficiency of the polarization matched light employing the proposed PSTE at three different primary colors, and it is compared with the extraction efficiency employing lossless ITO with refractive index of 1.94. Geometric parameters of PSTE were assumed as $t_z = 100$ nm, $t_x = t_y = 30$ nm, $P_x = 70$ nm, and $P_y = 800$ nm. As can be seen in Fig. 7(c), degradations of the extraction efficiency were below 14 percent point for all the primary color wavelength range.

IV. Conclusion

The PSTE having dual functions of transparent electrode and polarizer was proposed by adjusting the mesh size of the metal nano-wire transparent electrode. The transmittance of each polarization, ER and sheet resistance of the PSTE were evaluated with varying of geometrical parameters and wavelength. And, parametric studies have been carried out to give a guide for geometric parameter selection to meet the requirement of the target application. As an application of the PSTE, the way to reduce the 3D-crosstalk of passive stereoscopic 3D OLED display was also introduced by utilizing the PSTE instead of the conventional transparent electrode. The extraction efficiency of the proposed 3D OLED display pixel structure was also evaluated comparing with the conventional OLED pixel structure employing a lossless ITO. The author expects that the proposed PSTE can be not only an alternative of ITO material overcoming the drawback of high cost and limited supply of indium but also be the dual functional optoelectronic component which can be employed various application where polarization selectivity required at the transparent electrode layer.

References

[1] J. C. Su and T. M. Lin, "Polarized white light emitting diodes with a nano-wire grid polarizer," *Opt. Exp.*, vol. 21, no. 1, pp. 840–845, Jan. 2013.
[2] M. Ma *et al.*, "Polarized light emission from GaInN light-emitting diodes embedded with subwavelength aluminum wire-grid polarizers," *Appl. Phys. Lett.*, vol. 101, no. 6, Aug. 2012, Art. no. 061103.
[3] S. H. Kim, J. Park, and K. D. Lee, "Fabrication of a nano-wire grid polarizer for brightness enhancement in liquid crystal display," *Nanotechnology*, vol. 17, no. 17, pp. 4436–4438, Aug. 2006.
[4] Z. Ge and S. T. Wua, "Nanowire grid polarizer for energy efficient and wide-view liquid crystal displays," *Appl. Phys. Lett.*, vol. 93, no. 12, Sep. 2008, Art. no. 121104.

[5] C. Pentico, E. Gardner, D. Hansen, and R. Perkins, "New, high performance, durable polarizers for projection displays," *SID Symp. Dig. Tech. Papers*, vol. 32, no. 1, 2001, pp. 1287–1289.
[6] X. J. Yu and H. S. Kwok, "Application of wire-grid polarizers to projection displays," *Appl. Opt.,* vol. 42, no. 31, pp. 6335–6341, Nov. 2003.
[7] J. B. Young, H. A. Graham, and E. W. Peterson, "Wire grid infrared polarizer," *Appl. Opt.*, vol. 4, no. 8, pp. 1023–1026, Aug. 1965.
[8] Z. Y. Yang *et al.*, "Broadband polarizers using dual-layer metallic nanowire grids," *IEEE Photon. Technol. Lett.,* vol. 20, no. 9, pp. 697–699, May 2008.
[9] K. Takano, H. Yokoyama, A. Ichii, I. Morimoto, and M. Hangyo, "Wire-grid polarizer sheet in the terahertz region fabricated by nanoimprint technology," *Opt. Lett.,* vol. 36, no. 14, pp. 2665–2667, Jul. 2011.
[10] D. S. Hecht, L. Hu, and G. Irvin, "Emerging transparent electrodes based on thin films of carbon nanotubes, graphene, and metallic nanostructures," *Adv. Mater.*, vol. 23, no. 13, pp. 1482–1513, Feb. 2011.
[11] D. R. Cairns *et al.*, "Strain-dependent electrical resistance of tin-doped indium oxide on polymer substrates," *Appl. Phys. Lett.*, vol. 76, no. 11, pp. 1425–1427, Mar. 2000.
[12] D. R. Cairns and G. P. Crawford, "Electromechanical properties of transparent conducting wsubstrates for flexible electronic displays," *Proc. IEEE*, vol. 93, no. 8, pp. 1451–1458, Aug. 2005.
[13] K. Ellmer, "Past achievements and future challenges in the development of optically transparent electrodes," *Nature Photon.*, vol. 6, no. 12, pp. 809–817, Nov. 2012.
[14] T. B. Song and N. Li, "Emerging transparent conducting electrodes for organic light emitting diodes," *Electronics*, vol. 3, no. 1, pp. 190–204, Mar. 2014.
[15] Z. Wu *et al.*, "Transparent, conductive carbon nanotube films," *Science*, vol. 305, no. 27, pp. 1273–1276, Aug. 2004.
[16] M. Zhang *et al.*, "Strong, transparent, multifunctional, carbon nanotube sheets," *Science*, vol. 309, no. 5738, pp. 1215–1219, Aug. 2005.
[17] M. S. Lee *et al.*, "High-performance, transparent and stretchable electrodes using graphene-metal nanowire hybrid structures," *Nano Lett.*, vol. 13, no. 6, pp. 2814–2821, Jun. 2013.
[18] K. Rana, J. Singh, and J. H. Ahn, "A graphene-based transparent electrode for use in flexible optoelectronic devices," *J. Mater. Chem. C*, vol. 2, no. 15, pp. 2646–2656, Jan. 2014.
[19] S. Pang, Y. Hernandez, X. Feng, and K. Müllen, "Graphene as transparent electrode material for organic electronics," *Adv. Mater.*, vol. 23, no. 25, pp. 2779–2795, Apr. 2011.
[20] J. Wu *et al.*, "Organic light-emitting diodes on solution-processed graphene transparent electrodes," *ACS Nano*, vol. 4, no. 1, pp. 43–48, Nov. 2010.
[21] X. Wang, L. Zhi, and K. Müllen, "Transparent, conductive graphene electrodes for dye-sensitized solar cells," *Nano Lett.*, vol. 8, no. 1, pp. 323–327, Jan. 2008.
[22] M. G. Kang and L. J. Guo, "Nanoimprinted semitransparent metal electrodes and their application in organic light-emitting diodes," *Adv. Mater.*, vol. 19, no. 10, pp. 1391–1396, Apr. 2007.
[23] M. G. Kang, H. J. Park, S. H. Ahn, and L. J. Guo, "Transparent Cu nanowire mesh electrode on flexible substrates fabricated by transfer printing and its application inorganic solar cells," *Sol. Energy Mater. Sol. Cells*, vol. 94, no. 6, pp. 1179–1184, Mar. 2010.
[24] M. G. Kang, M. S. Kim, J. Kim, and L. J. Guo, "Organic solar cells using nanoimprinted transparent metal electrodes," *Adv. Mater.*, vol. 20, no. 23, pp. 4408–4413, Dec. 2008.
[25] M. G. Kang, H. J. Park, S. H. Ahn, T. Xu, and L. J. Guo, "Toward lowcost, high-efficiency, and scalable organic solar cells with transparent metal electrode and improved domain morphology," *IEEE J. Sel. Top. Quantum Electron.*, vol. 16, no. 6, pp. 1807–1820, Apr. 2010.
[26] J. Y. Lee, S. T. Connor, Y. Cui, and P. Peumans, "Solution-processed metal nanowire mesh transparent electrodes," *Nano Lett.*, vol. 8, no. 2, pp. 689–692, Feb. 2008.
[27] L. Hu, H. S. Kim, J. Y. Lee, P. Peumans, and Y. Cui, "Scalable coating and properties of transparent, flexible, silver nanowire electrodes," *ACS Nano*, vol. 4, no. 5, pp. 2955–2963, May, 2010.
[28] W. Gaynor, G. F. Burkhard, M. D. McGehee, and P. Peumans, "Smooth nanowire/polymer composite transparent electrodes," *Adv. Mater.*, vol. 23, no. 26, pp. 2905–2910, Apr. 2011.
[29] F. Afshinmanesh, A. G. Curto, K. M. Milaninia, N. F. van Hulst, and M. L. Brongersma, "Transparent metallic fractal electrodes for semiconductor devices," *Nano Lett.*, vol. 14, no. 9, pp. 5068–5074, Sep. 2014.
[30] H. Kang *et al.*, "A novel polarizer glasses-type 3D displays with a patterned retarder," *SID Symp. Dig. Tech. Papers*, vol. 41, no. 1, pp. 1–4, Jul. 2010.
[31] Y. J. Lim *et al.*, "Film patterned retarder for stereoscopic three-dimensional display using ink-jet printing method," *Opt. Exp.*, vol. 22, no. 19, pp. 22661–22666, Sep. 2014.
[32] M. B. Heaney, "Electrical conductivity and resistivity," in *Electrical Measurement in Signal Processing, and Displays*, ch. 7, Boca Raton, FL, USA: CRC Press, 2003, pp. 7–8.
[33] D. R. Lide, "Properties of solids," in *CRC Handbook of Chemistry and Physics*. Boca Raton, FL, USA: CRC Press, 2005, pp. 43–47.
[34] R. Bel Hadj Tahar, T. Ban, Y. Ohya, and Y. Takahashi, "Tin doped indium oxide thin films: Electrical properties," *J. Appl. Phys.*, vol. 83, no. 5, pp. 2631–2645, Mar. 1998.
[35] A. J. Woods, "Crosstalk in stereoscopic displays: A review," *J. Electron. Imag.*, vol. 21, no. 4, Dec. 2012, Art. no. 040902.
[36] A. D. Rakić, A. B. Djurišic, J. M. Elazar, and M. L. Majewski, "Optical properties of metallic films for vertical-cavity optoelectronic devices," *Appl. Opt.*, vol. 37, no. 22, pp. 5271–5283, Aug. 1998.